Acta Crystallographica Section B
Structural Science
ISSN 0108-7681

Two-dimensional incommensurately modulated structure of $(Sr_{0.13}Ca_{0.87})_2CoSi_2O_7$ crystals

B. Bagautdinov,[a] K. Hagiya,[a] K. Kusaka,[a] M. Ohmasa[a]* and K. Iishi[b]

[a]Department of Life Science, Himeji Institute of Technology, 3-2-1 Koto, Kamigori-cho, Ako-gun, Hyogo 678-1297, Japan, and [b]Department of Mineralogical Science and Geology, Yamaguchi University, Yoshida, Yamaguchi 753-0841, Japan

Correspondence e-mail: ohmasa@sci.himeji-tech.ac.jp

Received 18 April 2000
Accepted 3 May 2000

The incommensurate structure of $(Sr_{0.13}Ca_{0.87})_2CoSi_2O_7$ at room temperature has been determined from single-crystal X-ray diffraction data. The compound has a non-centrosymmetric tetragonal basic cell of a = 7.8743 (4) and c = 5.0417 (2) Å with the space group $P\bar{4}2_1m$. The refinements of the basic structure converged to R = 0.038 for 757 main reflections. The two-dimensional incommensurate structure is characterized by the wavevectors $\mathbf{q}_1 = 0.286\,(3)(\mathbf{a}^* + \mathbf{b}^*)$ and $\mathbf{q}_2 = 0.286\,(3)(-\mathbf{a}^* + \mathbf{b}^*)$, where $\mathbf{a}^*$, $\mathbf{b}^*$ are the reciprocal lattice vectors of the basic structure. With the (3 + 2)-dimensional superspace group $P^{P\bar{4}2_1m}_{p4mg}$, the refinements converged to R = 0.071 for 1697 observed reflections (757 main and 940 satellite reflections). The structure is described in terms of displacement of the atoms, rotation, distortion of CoO_4 and SiO_4 tetrahedra, and the partial ordering of the Sr and Ca atoms accompanied with the modulation. Correlated evolution of these features throughout the crystal gives rise to various oxygen coordination around Ca/Sr. Comparison of the derived modulated structure to that of $Ca_2CoSi_2O_7$ clarified that the partial substitution of Ca by large alkaline-earth atoms such as Sr should decrease the distortion of the polyhedra around the cations.

1. Introduction

$(Sr_{0.13}Ca_{0.87})_2CoSi_2O_7$ belongs to the family of melilite-type compounds of general stoichiometry $A_2T^1T^2{}_2O_7$, where A is a large eight-coordinated cation (A = Ca, Sr, Na, Ba, La), and T^1 and T^2 are small cations in a tetrahedral coordination (T^1 = Co, Mg, Fe, Cr, Zn, Al,...; T^2 = Si, Ge, Ga, Be,...). These compounds have been extensively studied for their two-dimensional incommensurate structures at ambient temperature and for their phase transition to normal phase at heating and to commensurate structure at cooling (Hemingway *et al.*, 1986; Seifert *et al.*, 1987; Riester & Böhm, 1997).

The structural principles of these materials are illustrated with the corner-sharing T^1O_4 tetrahedra and $T^2{}_2O_7$ tetrahedral dimers which are linked together and form irregular five-membered rings. The tetrahedral sheets have parallel orientation along (001), the interstices formed with two five-membered rings in adjacent layers are filled by A cations located halfway between the sheets (Smith, 1953). However, the actual structure of these compounds is more complex. A number of melilites adopts the incommensurate modulation in their structures and many of them have not yet been completely elucidated. It was supposed that a misfit between the sizes of interlayer cations A and the large space for A formed by the tetrahedral sheets might be responsible for the modulation in åkermanites (Hemingway *et al.*, 1986; Seifert *et*

al., 1987). A change in the structural misfit by isomorphous substitution as well as a variation in temperature affects the length of the modulation vectors. Expansion of dimensions of the tetrahedral sheet, *i.e.* the size of pentagonal holes, stabilizes the low-temperature structural variants, and contrarily the increase in size of *A* cations stabilizes the high-temperature structural variants (Röthlisberger *et al.*, 1990; Armbruster *et al.*, 1990).

The modulated structure of Co-åkermanite, $Ca_2CoSi_2O_7$, was determined by Hagiya *et al.* (1993) based on the refinements in the (3 + 2)-dimensional space. They clarified that the modulation is caused by the shifts of the constituent atoms and the coordination number of Ca varies from eight to six in the structure. The influence of substitution of Mg by Fe in tetrahedral sheets on the modulated structure of $Ca_2(Mg_{0.55},Fe_{0.45})Si_2O_7$ was investigated by Kusaka *et al.* (1998). The modulated structure of the Mg end-member $Ca_2MgSi_2O_7$ was also analysed (Kusaka, 1999).

Electron diffraction patterns of $(Sr_xCa_{1-x})_2CoSi_2O_7$ solid solutions, where some of the interlayer Ca cations are substituted by large Sr, shows satellite reflections at room temperature in the range x = 0.0–0.3 (Iishi *et al.*, 1990). Sharpness and intensity of the satellites continuously decrease with an increase in Sr content. Circular diffuse scattering connecting the satellites was also observed in the diffraction patterns of the solid solution (Iishi *et al.*, 1990, 1994). No structural study of the incommensurate phase of these compounds has been performed and the effects of substitution at the *A* site on the modulation are still left unknown.

This paper deals with the detailed examination, based on a (3 + 2)-dimensional superspace formalism (de Wolff *et al.*, 1981), of the two-dimensional incommensurately modulated structure of $(Sr_{0.13}Ca_{0.87})_2CoSi_2O_7$. Comparison between the modulated structures of $(Sr_{0.13}Ca_{0.87})_2CoSi_2O_7$ and $Ca_2CoSi_2O_7$ (Hagiya *et al.*, 1993; Kusaka, 1999) allows the discovery of peculiarities in the substitution of the interlayer Ca atoms by larger Sr.

2. Experimental

$(Sr_{0.13}Ca_{0.87})_2CoSi_2O_7$ single crystals were grown in nitrogen gas by the floating zone method. Details of the synthesis are described by Iishi *et al.* (1990). A spherical sample (r = 0.15 mm) was mounted on a four-circle diffractometer (Enraf–Nonius CAD-4) with graphite-monochromated Mo $K\alpha$ radiation (λ = 0.71073 Å). Since the absorption of Mo $K\alpha$ radiation in $(Sr_{0.13}Ca_{0.87})_2CoSi_2O_7$ is not high (μ = 6.739 mm^{-1}), this relatively large specimen was found to be more suitable to collect weak intensities of the satellite reflections. The lattice constants of the basic structure unit cell were refined by a least-squares method with angular data of 25 main reflections in the range $14 < \theta < 33°$. Details of the experiment and the refinement are summarized in Table 1.[1]

[1] Supplementary data for this paper are available from the IUCr electronic archives (Reference: SN0002). Services for accessing these data are described at the back of the journal.

Table 1
Experimental details.

Crystal data	
Chemical formula	$(Sr_{0.13}Ca_{0.87})_2CoSi_2O_7$
Chemical formula weight	319.6
Temperature (K)	293
Cell setting	Tetragonal
Superspace group	$P^{P\bar{4}2_1m}_{p4mg}$
a (Å)	7.8743 (4)
c (Å)	5.0417 (2)
V (Å^3)	312.61 (3)
Formula units (Z)	2
D_x (Mg m^{-3})	3.394
Modulation wavevectors	$\mathbf{q}_1$ = 0.286 (3)($\mathbf{a}^*$ + $\mathbf{b}^*$)
	$\mathbf{q}_2$ = 0.286 (3)($-\mathbf{a}^*$ + $\mathbf{b}^*$)
Modulation period (Å)	λ = 19.41 (3)
Crystal form	Sphere
Crystal size (mm)	r = 0.15
Crystal colour	Blue
Data collection	
Diffractometer	Enraf–Nonious CAD-4
Radiation type	Mo $K\alpha$
Wavelength (Å)	0.71073
$\Delta f'$, f'' Sr	−1.531, 3.250
$\Delta f'$, f'' Ca	0.226, 0.306
$\Delta f'$, f'' Co	0.349, 0.972
$\Delta f'$, f'' Si	0.082, 0.070
$\Delta f'$, f'' O	0.011, 0.006
Absorption correction type	Analytical
Transmission extremes T_{min}/T_{max}	0.2249/0.2733
Absorption coefficient μ (mm^{-1})	6.739
Range of h, k, l	$0 \rightarrow h \rightarrow 10$
	$0 \rightarrow k \rightarrow 15$
	$0 \rightarrow l \rightarrow 10$
	$-1 \rightarrow m \rightarrow 1$
	$-1 \rightarrow n \rightarrow 1$
Standard reflection/maximum deviation	(7,3,0)/1.3%; (−3,7,0)/1.5%
No. of unique reflections	8207
No. of observed reflections	1697
No. of main reflections	757
No. of satellites	940
with (m,n) equal to ±(1,0), ±(0,1)	730
with (m,n) equal to ±(1,1), ±(−1,1)	210
Criterion for observed reflections	$I > 2.5\sigma(I)$
Refinement	
Refinement on	F
R, wR (all reflections)	0.070, 0.052
R, wR (main reflections)	0.037, 0.036
R, wR (satellites)	
for ±(1,0), ±(0,1)	0.219, 0.262
for ±(1,1), ±(−1,1)	0.314, 0.378
S	2.34
No. of parameters	107
Weighting scheme	w = 1
$(\Delta/\text{s.u.})_{max}$	1.147
$\Delta\rho_{max}$ (e Å^{-3})	2.59
$\Delta\rho_{min}$ (e Å^{-3})	−2.94
Extinction method	Isotropic type I (Becker & Coppens, 1974)
Extinction coefficient	0.102 (9)
Source of atomic scattering factors	*International Tables for X-ray Crystallography* (1992, Vol. C)

With respect to the reciprocal cell basis ($\mathbf{a}^*$, $\mathbf{b}^*$, $\mathbf{c}^*$) all reflections on diffraction patterns could be indexed with five integers

$$S = h\mathbf{a}^* + k\mathbf{b}^* + l\mathbf{c}^* + m\mathbf{q}_1^* + n\mathbf{q}_2^*.$$

The components of the modulation wavevectors are $\mathbf{q}_1 = (\alpha, \alpha, 0)$ and $\mathbf{q}_2 = (-\alpha, \alpha, 0)$. From the positions of 11 satellite

reflections, the variable α = 0.286 (3) was determined. Each main reflection is surrounded by eight satellites, which have the indices *hklmn*, where (*m*, *n*) are ±(1,0), ±(0,1), ±(1,1), ±(−1,1). The integrated intensities up to the scattering angle $\theta = 47.33^\circ$ were measured for the main reflections and for the above-mentioned eight satellites assigned to each main reflection. From this data set, the reflections with intensities larger than 2.5 times their standard deviation were selected for the structure determination. Analysis of the data by the indexing shows that there are 757 main and 940 first-order satellite reflections. Higher-order satellites were not detected, but the circular diffuse scattering was observed in the precession photographs. This is coincidental to the observation of electron diffraction patterns of $(Sr_xCa_{1-x})_2CoSi_2O_7$ solid solutions, where only weak first-order satellites were found with Sr content ∼0.15 (Iishi *et al.*, 1990). Intensities were corrected for Lorentz, polarization and absorption factors with the *DATRED* program of the *JANA*98 computing system (Petricek & Dusek, 1998).

3. Symmetry and refinements

The space group of the åkermanite structure is $P\bar{4}2_1m$ (Smith, 1953). The reflection conditions of the diffraction patterns for the main reflections (*h*0000), with *h* even, and for the satellites ($h00m\bar{m}$), with *h* even, (*hhlm*0), with *m* even, of $(Sr_{0.13}Ca_{0.87})_2CoSi_2O_7$ are the same as those in $Ca_2CoSi_2O_7$ (Hagiya *et al.*, 1993) and $Ca_2(Mg_{0.55},Fe_{0.45})Si_2O_7$ (Kusaka *et al.*, 1998). Therefore, the same superspace group $P^{P\bar{4}2_1m}_{p4mg}$ was chosen in the present study. For a description of the incommensurate structure of $(Sr_{0.13}Ca_{0.87})_2CoSi_2O_7$ in (3 + 2)-dimensional superspace, two types of modulation waves have to be introduced: the waves for the displacive modulations describing displacements of all the atoms and the density modulation characterizing the occupancy probability of Sr and Ca atoms.

The position of the μth atom in a two-dimensionally modulated structure is given as the sum of a translational, symmetric, basic structure position $\mathbf{r}^\mu = (\bar{x}, \bar{y}, \bar{z})$ and a modulation function $\mathbf{U}^\mu(\bar{x}_4, \bar{x}_5)$ representing displacement of the atom

$$\mathbf{r}^\mu(\overline{x}_4, \overline{x}_5) = \mathbf{r}^\mu + \mathbf{U}^\mu(\overline{x}_4, \overline{x}_5),$$

where $\mathbf{r}^\mu = \mathbf{p} + \mathbf{r}_0{}^\mu$, where $\mathbf{p}$ is a direct-lattice vector and $\mathbf{r}_0^\mu$ determines the position of the μth atom in a unit cell. The arguments $\bar{x}_4$ and $\bar{x}_5$ are defined as

$$\overline{x}_4 = \mathbf{q}_1\mathbf{r}^\mu + t_1$$
$$\overline{x}_5 = \mathbf{q}_2\mathbf{r}^\mu + t_2,$$

where $\mathbf{q}_1$ and $\mathbf{q}_2$ are the modulation vectors, and t_1 and t_2 are the internal phases. Owing to the periodicity of the modulation, the components of the displacement of each atom can be expressed as an expansion of a Fourier series

Table 2
Site-occupancy factors, fractional atomic coordinates and equivalent isotropic atomic displacement parameters (Å^2) of the basic structure of $(Sr_{0.13}Ca_{0.87})_2CoSi_2O_7$.

Standard uncertainties are given in parentheses. Parameters without standard uncertainties are dependent on other parameters.

$$U_{\rm eq} = (1/3)\sum_i\sum_j U^{ij}a_i^*a_j^*\mathbf{a}_i\mathbf{a}_j$$

	Occ.	*x*	*y*	*z*	$U_{\rm eq}$
Sr	0.128	0.33234	1/2 − *x*	0.5058	0.01845
Ca	0.872 (3)	0.33234 (4)	1/2 − *x*	0.5058 (1)	0.01845 (8)
Co	1	0	0	0	0.01184 (7)
Si	1	0.13915 (7)	1/2 − *x*	0.9382 (1)	0.0113 (1)
O(1)	1	0	1/2	0.8254 (6)	0.0354 (8)
O(2)	1	0.1401 (2)	1/2 − *x*	0.2547 (4)	0.0244 (4)
O(3)	1	0.0798 (3)	0.1894 (2)	0.7863 (3)	0.0289 (5)

$$U^\mu_\alpha(\overline{x}_4, \overline{x}_5) = \sum_{n_1}\sum_{n_2} A^\mu_{n_1n_2\alpha}\cos(2\pi n_1\overline{x}_4 + 2\pi n_2\overline{x}_5) + B^\mu_{n_1n_2\alpha}\sin(2\pi n_1\overline{x}_4 + 2\pi n_2\overline{x}_5),$$

where (n_1 and n_2) define the order of the Fourier terms, and $\alpha = x$, y, z. The position $\mathbf{r}_0^\mu$ is defined by $\mathbf{r}_0^\mu = \mathbf{r}_\mathbf{b}^\mu + \sum_{\alpha=1}^3 A^\mu_{00\alpha}\mathbf{a}_\alpha$, where $\mathbf{a}_\alpha$ are the basic lattice vectors, $\mathbf{r}_\mathbf{b}^\mu$ is the position of the atoms in the basic cell determined using the main reflection data, and $A^\mu_{00\alpha}$ are the zeroth-order Fourier terms.

The occupation probability of Sr and Ca atoms at the *A* site is described by a scalar function $P'^\mu(\overline{x}_4, \overline{x}_5) = P_0 + P^\mu(\overline{x}_4, \overline{x}_5)$, where $P_0 = \langle P'^\mu(\overline{x}_4, \overline{x}_5)\rangle$ is the average occupation. Supposing that these two types of atoms are distributed to the *A* site without vacancies, the relevant occupancy probabilities to them are $P'^\mu(\overline{x}_4, \overline{x}_5)$ and $1 - P'^\mu(\overline{x}_4, \overline{x}_5)$, respectively. The components of $P'^\mu(\overline{x}_4, \overline{x}_5)$ are also expanded in terms of a Fourier series

$$P^\mu(\overline{x}_4, \overline{x}_5) = \sum_{n_1}\sum_{n_2} A^\mu_{n_1n_2}\cos(2\pi n_1\overline{x}_4 + 2\pi n_2\overline{x}_5) + B^\mu_{n_1n_2}\sin(2\pi n_1\overline{x}_4 + 2\pi n_2\overline{x}_5).$$

As only the first-order satellites are measured, Fourier amplitudes up to the orders $n_1 = 1$ and $n_2 = 1$ were used for the structure analysis. The symmetry restrictions imposed on the Fourier terms, $\mathbf{U}^\mu_\alpha$ and P^μ, of the atoms at the special positions in the basic structure are presented in Table 4. Refinements were performed using the system of computer programs *JANA*98 (Petricek & Dusek, 1998). The (3 + 2)-dimensional modulation parameters as a function of the t_1 and t_2 coordinates were calculated with a program written by K. Hagiya (unpublished).

3.1. The basic structure

The structure of $(Sr_{0.13}Ca_{0.87})_2CoSi_2O_7$ was refined using only the main reflections and the atomic positions of the basic structure of $Ca_2CoSi_2O_7$ (Hagiya *et al.*, 1993) as the starting parameters. The occupancy for Sr and Ca atoms at the *A* site

Table 3
Anisotropic atomic displacement parameters ($\times 10^4$ Å^2) and relative anisotropy of thermal ellipsoids E_{min}/E_{max} of the $(Sr_{0.13}Ca_{0.87})_2CoSi_2O_7$ structure.

Standard uncertainties are shown in parentheses. The temperature factor is defined by

$$\exp -2\pi^2[U^{11}h^2(\mathbf{a}^*)^2 + U^{22}k^2(\mathbf{b}^*)^2 + U^{33}l^2(\mathbf{c}^*)^2 + 2U^{12}hk(\mathbf{a}^*\mathbf{b}^*) + 2U^{13}hl(\mathbf{a}^*\mathbf{c}^*) + 2U^{23}kl(\mathbf{a}^*\mathbf{c}^*)].$$

E_{min}/E_{max} is the ratio of the smallest and largest eigenvalues.

		U^{11}	U^{22}	U^{33}	U^{12}	U^{13}	U^{23}	E_{min}/E_{max}
Ca/Sr	*b*	221 (1)	U^{11}	111 (1)	108 (1)	$-U^{23}$	−16 (1)	0.59 (2)
	m	199 (2)	U^{11}	100 (2)	89 (2)	$-U^{23}$	−15 (1)	0.62 (3)
Co	*b*	121 (1)	U^{11}	113 (1)	0	0	0	0.97 (2)
	m	109 (1)	U^{11}	109 (1)	0	0	0	1.0 (2)
Si	*b*	126 (2)	U^{11}	86 (2)	16 (2)	$-U^{23}$	−5 (1)	0.88 (3)
	m	112 (2)	U^{11}	76 (2)	14 (2)	$-U^{23}$	0 (1)	0.87 (3)
O(1)	*b*	480 (16)	U^{11}	84 (9)	350 (16)	0	0	0.42 (9)
	m	450 (16)	U^{11}	70 (9)	330 (16)	0	0	0.41 (9)
O(2)	*b*	325 (7)	U^{11}	81 (6)	150 (10)	$-U^{23}$	14 (4)	0.61 (9)
	m	303 (8)	U^{11}	73 (7)	140 (10)	$-U^{23}$	17 (5)	0.67 (9)
O(3)	*b*	540 (10)	167 (6)	164 (5)	−131 (7)	99 (7)	−23 (5)	0.60 (8)
	m	420 (10)	155 (6)	141 (8)	−120 (7)	64 (8)	−14 (6)	0.63 (8)

b = basic structure; *m* = modulated structure.

Table 4
Fractional Fourier amplitudes ($\times 10^3$) of the modulation functions with standard uncertainties in parentheses.

Symmetry restrictions on the parameters of the modulation functions are shown.

		$A_{00\alpha}$, P_0	$A_{10\alpha}$	$A_{11\alpha}$	$A_{01\alpha}$	$A_{-11\alpha}$	$B_{10\alpha}$	$B_{11\alpha}$	$B_{01\alpha}$	$B_{-11\alpha}$
Ca/Sr	U_x	−0.01 (4)	3.5 (1)	−0.9 (2)	4.4 (1)	−1.3 (2)	0.6 (1)	3.1 (2)	1.6 (1)	−4.2 (2)
	U_y	$-A_{00x}$	A_{10x}	$-A_{-11x}$	A_{01x}	$-A_{11x}$	$-B_{10x}$	B_{-11x}	B_{01x}	$-B_{11x}$
	U_z	−0.03 (1)	0	2.2 (4)	0	A_{11z}	6.5 (3)	5.8 (3)	0	B_{11z}
	P^{Sr}	126 (3)	0	−9 (6)	0	−9 (6)	59 (4)	−2 (6)	0	−2 (6)
	P^{Ca}	$1 - P_{00}^{Sr}$	0	$-A_{11}^{Sr}$	0	$-A_{-11}^{Sr}$	$-B_{10}^{Sr}$	$-B_{11}^{Sr}$	0	$-B_{-11}^{Sr}$
Co	U_x	0	0	0	0	0	−2.6 (1)	2.3 (2)	4.4 (1)	−1.3 (2)
	U_y	0	0	0	0	0	$-B_{01x}$	$-B_{-11x}$	B_{10x}	B_{11x}
	U_z	0	1.8 (2)	1.4 (4)	$-A_{10z}$	$-A_{11z}$	0	0	0	0
Si	U_x	0.00 (2)	3.7 (2)	−1.8 (4)	1.0 (1)	1.8 (4)	3.6 (2)	−0.8 (3)	0.4 (2)	−0.7 (3)
	U_y	$-A_{00x}$	A_{10x}	$-A_{-11x}$	A_{01x}	$-A_{11x}$	$-B_{10x}$	B_{-11x}	B_{01x}	$-B_{11x}$
	U_z	0.01 (1)	0	3.5 (6)	0	A_{11z}	5.6 (4)	0.9 (5)	0	B_{11z}
O(1)	U_x	0.00 (2)	0	0	0	0	2.8 (8)	2.0 (2)	−0.7 (1)	−0.3 (2)
	U_y	0	0	0	0	0	$-B_{10x}$	$-B_{-11x}$	B_{01x}	$-B_{11x}$
	U_z	−0.01 (4)	0	−0.5 (3)	0	A_{11z}	0	0	0	0
O(2)	U_x	0.00 (2)	5.1 (6)	1 (1)	3.0 (6)	−5 (1)	0.6 (5)	−3 (1)	2.0 (6)	3 (1)
	U_y	$-A_{00x}$	A_{10x}	$-A_{-11x}$	A_{01x}	$-A_{11x}$	$-B_{10x}$	B_{-11x}	B_{01x}	$-B_{11x}$
	U_z	−0.01 (4)	0	5 (2)	0	A_{11z}	4 (1)	2 (1)	0	B_{11z}
O(3)	U_x	−0.02 (5)	6.8 (7)	5 (1)	3.7 (7)	12 (2)	1.5 (7)	5 (1)	5.8 (6)	−2 (1)
	U_y	0.00 (2)	0.7 (5)	2 (1)	−1.0 (3)	6 (8)	−3.8 (5)	−2 (1)	−1.6 (2)	2 (1)
	U_z	−0.02 (2)	5.3 (9)	−6 (2)	2.0 (4)	10 (2)	5 (1)	0 (1)	2.3 (3)	−3 (2)

without a vacancy was applied. The refinement for the non-centrosymmetric space group $P\bar{4}2_1m$, using 757 main reflections, led to $R(F) = 0.038$ and $wR(F) = 0.036$. A total number of 36 independent parameters, including anisotropic displacement parameters for all atoms and an occupancy parameter for the *A* site, were used for the refinements. The final refined occupancy, fractional coordinates and components of the temperature tensors are given in Tables 2 and 3. The structure projected onto the (001) plane is shown in Fig. 1.

3.2. The incommensurate structure

The atomic positions of the basic structure were used as the initial parameters for the refinement of the modulated structure. The complementary occupancy probabilities of Ca and Sr atoms at the *A* site were introduced. The positional, thermal and modulation parameters of Ca and Sr atoms were held equal. All data of the main and satellite reflections were used for the refinements. Since the whole satellites have a weak intensity, a unitary weighting scheme was used during the refinements to give sufficient weight to the satellite reflections. Refinements for the (3 + 2)-dimensional space group $P^{P\bar{4}2_1m}_{p4mg}$, reduced $R(F)$ to 0.071 for all 1697 reflections, $R(F)$ = 0.037 for 757 main reflections, $R(F)$ = 0.219 for 730 satellites with (m, n) equal to $\pm(0,1)$ and $\pm(1,0)$, and $R(F)$ = 0.313 for 210 satellites with (m, n) equal to $\pm(1,1)$ and $\pm(-1,1)$. A total number of 107 independent parameters were refined. The final agreement factors for the satellites are rather high, but this can be explained by the fact that most satellites are very weak and many of them are just above the lowest level of observation. Therefore, errors of their intensities should be high. Moreover, the circular diffuse scattering overlapping with the satellites was observed in the diffraction patterns and the high *R* factors for them should also be attributed to the difficulties in accurate separation of the satellites from the diffuse streaks. Especially the satellites with (m, n) equal to $\pm(1,1)$ and $\pm(-1,1)$ were not fitted well by least-squares refinements, but the presence of these satellites in the reflection data improved the stability of the fit. The thermal displacement parameters, displacive and density modulation amplitudes as well as the occupancy parameters are listed in Tables 3 and 4.

4. Discussion

4.1. Description of the basic structure

The basic structure consists of tetrahedral layers of five-membered rings. The layers are stacked along [001] so as to form pentagonal channels parallel to the *c* axis (Fig. 1). The

structure is characterized by strong anisotropy of the displacement ellipsoids of the oxygen and Ca/Sr atoms (see Fig. 1 and Table 3). The longest axes of the ellipsoids lie almost in the (001) plane and are oriented towards the ⟨110⟩ direction, except the axis of O(3). The ratios of the minimum axial lengths (minimum eigenvalues) to the maximum ones (maximum eigenvalues) E_{min}/E_{max} are shown in Table 3. The forms of the ellipsoids of the Co and Si cations are almost spherical. The O(1) atom bridging the two tetrahedra in the Si_2O_7 dimer shows the largest anisotropy. The shifts of the O(1) atoms towards the center of the channels should be coupled with the displacement of the Ca/Sr atoms located in the channels, because the displacement directions of Ca/Sr and O(1) atoms are mutually perpendicular (Fig. 1). The disposition of the displacement tensors $\mathbf{U}^{ij}$ of the O atoms can be explained by rotations of the CoO_4 and SiO_4 tetrahedral units around [001]. In fact, all the O atoms have the largest eigenvalue axes perpendicular to the directions of the Co—O and Si—O bonds. The anomalously large displacement feature in the average structure probably reflects the amplitudes of the displacive modulation and the occupational disorder due to the substitution of Ca by Sr. The latter is reinforced by the observation of the diffuse scattering in the diffraction patterns.

Interatomic distances (Table 5) show that the *A*-site atom Ca/Sr is located in an eight-coordinate interstice and irregular Ca/Sr—O distances range from 2.446 (2) to 2.716 (2) Å. The average distance of 2.587 (2) Å is larger than the sum of the ionic radii of O^{2-} (r = 1.28 Å) and Ca^{2+} (r = 1.26 Å), but smaller in the case of Sr^{2+} (r = 1.40 Å; Shannon, 1976). Ca/Sr has four compressed bonds with $O(1)^{i}$, $O(2)^{ii}$, $O(3)^{ii}$ and $O(3)^{iv}$, and contrarily the remaining four bonds with $O(2)^{i}$, $O(2)^{iii}$, $O(3)^{i}$ and $O(3)^{iii}$ are stretched.

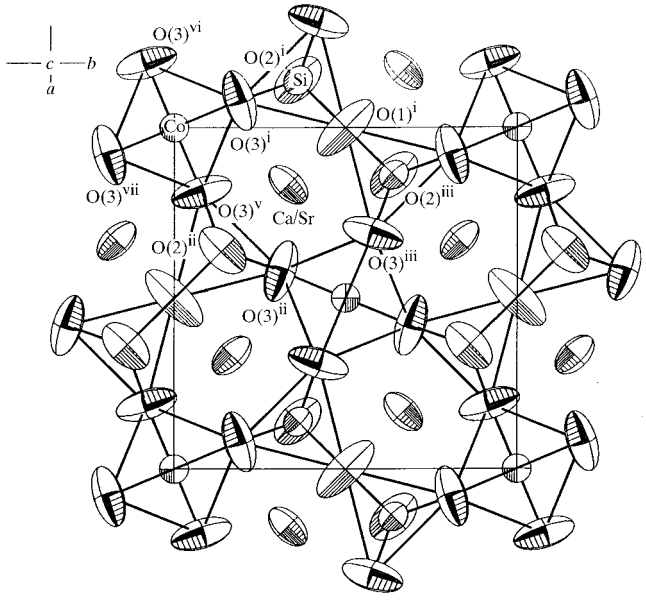

Figure 1
Projection of the basic structure of $(Sr_{0.13}Ca_{0.87})_2CoSi_2O_7$ onto the (001) plane. The atoms are represented by ellipsoids with 50% probability level. O—O connections are also shown to illustrate the tetrahedra of the Co and Si atoms.

The CoO_4 tetrahedron contains regular Co—O bonds which are equal to 1.944 (2) Å. However, the two relatively longer edges $O(3)^{i}$—$O(3)^{vii}$ and $O(3)^{v}$—$O(3)^{vi}$ parallel to (001), and larger angles $O(3)^{i}$—Co—$O(3)^{vii}$ and $O(3)^{v}$—Co—$O(3)^{vi}$ indicate that the CoO_4 tetrahedron is slightly flattened on (001) (see Fig. 1). The SiO_4 tetrahedron, being more distorted, contains a compressed Si—$O(2)^{viii}$ bond aligned in [001] and the angles have large deviations from the regular tetrahedral angle of 109.49°.

4.2. Description of the modulated structure

Details of the actual structure of the present material were obtained by the refinements of the modulated structure. Since parameters of each atom in the (3 + 2)-dimensional superspace representation can be considered as a continuous surface along the two internal directions t_1 and t_2, (t_1, t_2) plots are used to represent the atomic displacements, interatomic distances and other structural characteristics in the following discussion. Owing to the periodicity along the fourth and fifth coordinates in the superspace, all information about the structure is enclosed with the unit lengths of both t_1 and t_2. Any pair of (t_1, t_2) corresponds to a value of ($\bar{x}_4$, $\bar{x}_5$) in the structure.

The magnitudes of the Fourier components of the occupational probability of the Sr and Ca atoms at the *A* site show apparent ordering of the substituted atoms only along t_1 with a sinusoidal form and the other components are not significantly larger than their standard uncertainties (Table 4). Analysis of the density modulation revealed the occupancy of Sr at the *A* site to vary between 0.06 and 0.19 (Fig. 2). The occupancy of Ca changes accordingly between 0.94 and 0.81. The sinusoidal form of the occupancy modulation of Sr and Ca, which should normally be modelled on a rectangular form with height 1, may be ascribed to the disorder included in the crystal and detected as the circular diffuse scattering.

Although the refinements of the structure in the (3 + 2)-dimensional space reduced the size and anisotropy of the displacement ellipsoids of the atoms determined by the analysis of the basic structure, the orientational features of the ellipsoids are still unchanged, as listed in Table 3. The displacement range of all the atoms due to modulation is

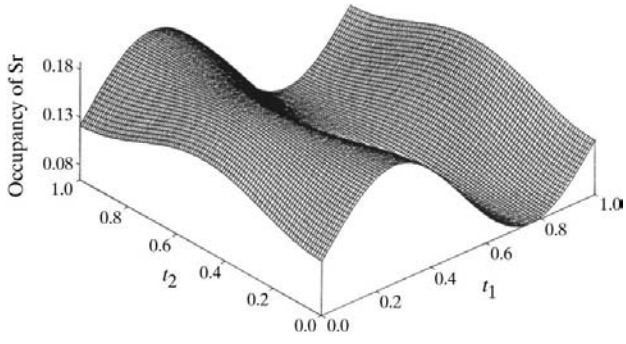

Figure 2
Distribution of the occupancy of the Sr atom at the *A* site of $(Sr_{0.13}Ca_{0.87})_2CoSi_2O_7$ *versus* t_1 and t_2.

Table 5
The interatomic distances (Å) and tetrahedral angles (°) of $(Sr_{0.13}Ca_{0.87})_2CoSi_2O_7$.

		Modulated structure		
	Basic structure	Minimal	Maximal	Variation
Ca/Sr—O polyhedra				
Ca/Sr—O(1)^{i}	2.505 (2)	2.435 (4)	2.584 (3)	0.149 (5)
Ca/Sr—O(2)^{ii}	2.487 (2)	2.474 (4)	2.505 (4)	0.030 (6)
Ca/Sr—O(2)^{i,iii}	2.716 (2)	2.560 (4)	2.816 (3)	0.256 (5)
Ca/Sr—O(3)^{ii,iv}	2.446 (2)	2.342 (4)	2.537 (4)	0.195 (6)
Ca/Sr—O(3)^{i,iii}	2.690 (2)	2.515 (4)	3.019 (4)	0.504 (6)
Average length	2.587 (2)	2.563 (4)	2.734 (4)	0.271 (6)
CoO_4 tetrahedra				
Co—O(3)^{i,v,vi,vii}	1.944 (2)	1.891 (5)	2.008 (4)	0.117 (6)
O(3)$^{i(vii)}$—O(3)$^{v,vi(v,vi)}$	3.142 (3)	3.052 (4)	3.222 (3)	0.170 (5)
O(3)$^{i(v)}$—O(3)$^{vii(vi)}$	3.235 (2)	3.174 (4)	3.341 (4)	0.167 (5)
O(3)$^{i(vii)}$—Co—O(3)$^{v,vi(v,vi)}$	107.88 (8)	104.41 (9)	110.57 (10)	6.16 (13)
O(3)$^{i(v)}$—Co—O(3)$^{vii(vi)}$	112.70 (7)	108.83 (8)	118.10 (7)	9.27 (10)
SiO_4 tetrahedra				
Si—O(1)^{ii}	1.651 (1)	1.619 (3)	1.682 (4)	0.063 (5)
Si—O(2)^{viii}	1.596 (2)	1.557 (4)	1.639 (4)	0.081 (6)
Si—O(3)^{ii,iv}	1.621 (2)	1.580 (3)	1.655 (4)	0.075 (5)
O(1)—O(2)^{viii}	2.669 (3)	2.660 (5)	2.686 (4)	0.026 (6)
O(1)—O(3)^{ii,iv}	2.533 (2)	2.452 (6)	2.604 (5)	0.152 (7)
O(2)^{viii}—O(3)^{ii,iv}	2.758 (2)	2.648 (4)	2.871 (5)	0.169 (6)
O(3)—O(3)^{iv}	2.571 (3)	2.502 (5)	2.639 (3)	0.137 (6)
O(1)—Si—O(2)^{viii}	110.54 (12)	109.16 (11)	111.95 (9)	2.79 (14)
O(1)—Si—O(3)^{ii,iv}	101.47 (9)	97.72 (10)	106.55 (10)	8.83 (14)
O(2)^{viii}—Si—O(3)^{ii,iv}	118.00 (9)	110.75 (12)	124.58 (9)	13.83 (14)
O(3)—Si—O(3)^{v}	104.92 (10)	102.20 (12)	107.65 (10)	5.45 (15)

Symmetry codes: (i) $y, -x, 1-z$; (ii) x, y, z; (iii) $\frac{1}{2}+x, \frac{1}{2}-y, 1-z$; (iv) $\frac{1}{2}-y, \frac{1}{2}-x, z$; (v) $x, y, -1+z$; (vi) $-x, -y, -1+z$; (vii) $-y, x, 1-z$; (viii) $x, y, 1+z$. x, y and z are the average atomic coordinates with space group $P\bar{4}2_1m$.

presented in Table 6(*a*). The values indicate that the components of the shifts of the atoms are mainly in the (001) plane and those for Ca/Sr, O(1) and O(3) are larger than the rest. The z coordinates of O(1) and Co practically do not change with t_1 and t_2, while those of Ca/Sr and O(3) change remarkably. The displacement of the O(1) atom along ⟨110⟩ causes a bend of the Si_2O_7 dimer towards the center of the pentagonal channel. Two SiO_4 tetrahedra in the Si_2O_7 dimer rotate in an opposite sense and the rotation results in a twist of the dimer. The variation range of the twist-angle was estimated to be ±6.2° with the deviation of the angle O(3)^{i}—O(1)^{i}—O(3)^{iii} from that in the basic structure (118.2°, see Fig. 3). It is worth pointing out that the occupancy probability of the *A* site by Sr is highest around the (t_1, t_2) area close to the area of large O(3)^{i}—O(1)^{i}—O(3)^{iii} angles, and contrarily the occupancy by Ca is high in the area corresponding to the smaller angles (see Figs. 2 and 3). Thus, the large size Sr atoms are accommodated in the likely interstices of the pentagonal channels and the occupation of Sr increase the O(3)^{i}—O(1)^{i}—O(3)^{iii} angle. The components of the displacive modulation of Ca/Sr atoms along ⟨110⟩, determined using the Fourier amplitudes, are displayed as functions of (t_1, t_2) in Fig. 4. The largest displacements in ⟨110⟩ are found at around (0,0), (0,1/2), (1/2,0), (0,1), (1,0), (1,1), (1,1/2) and (1/2,1) in the figure. These regions of the large displacements of Ca/Sr matched the region of the large twist angles in Fig. 3. This may be attributed to a combination of the displacements of Ca/Sr and O(1) atoms in perpendicular directions. The O(3) atoms of the Si_2O_7 dimer are also shared with CoO_4 tetrahedra and the twists of the dimer therefore impose rotations of the tetrahedra around ⟨001⟩. Fig. 5 indicates variation in the rotation angles of CoO_4 tetrahedra from the basic structure positions. The largest rotation angle is 5.68°.

The displacive modulations of the atoms cause variations in the interatomic distances throughout the structure (Table 5). The shorter bonds denoted as the compressed bonds of Ca/Sr—O polyhedra show less variation, while the longer bonds specified as the stretched ones show a larger variation.

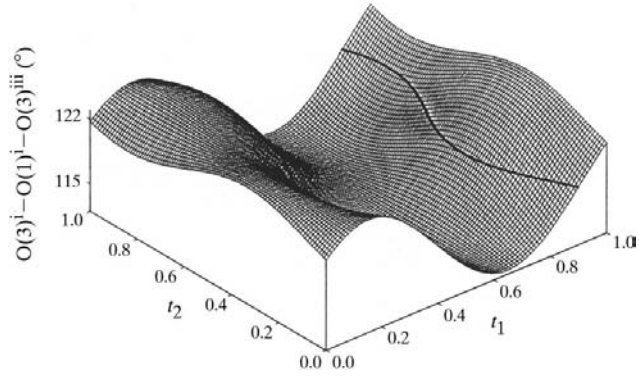

Figure 3
Variation of the twist angle of the Si_2O_7 dimer as a function of (t_1, t_2). The contours correspond to the O(3)^{i}—O(1)^{i}—O(3)^{iii} angle of 118.2° in the basic structure. Symmetry codes are shown in Table 5.

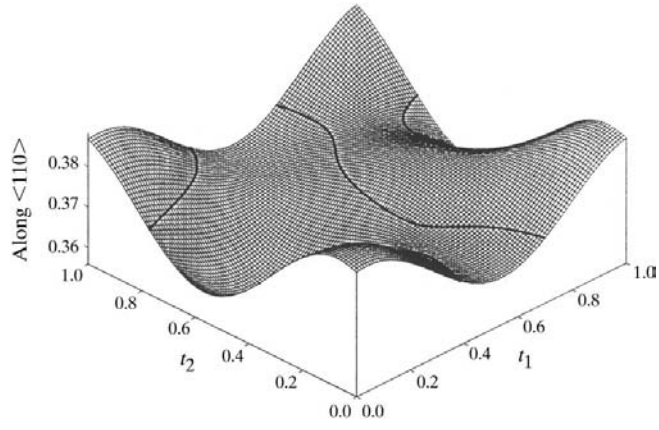

Figure 4
Displacive modulation of Ca/Sr along ⟨110⟩ as functions of t_1, t_2. The contour lines at 0.372 correspond to the ⟨110⟩ component in the basic structure.

Table 6
Atomic displacement range (Å) in modulated waves of the atoms.

Atoms	Along *a* axis	Along *b* axis	Along *c* axis	Maximum length of displacement
(*a*) $(Sr_{0.13}Ca_{0.87})_2CoSi_2O_7$				
Ca/Sr	0.201	0.201	0.141	0.317
Co	0.128	0.128	0.020	0.182
Si	0.120	0.120	0.061	0.180
O(1)	0.235	0.235	0.018	0.338
O(2)	0.189	0.189	0.091	0.282
O(3)	0.306	0.121	0.235	0.492
(*b*) $Ca_2CoSi_2O_7$†				
Ca	0.593	0.593	0.198	0.862
Co	0.292	0.292	0.076	0.420
Si	0.280	0.280	0.163	0.428
O(1)	0.720	0.720	0.123	1.026
O(2)	0.442	0.442	0.174	0.649
O(3)	1.016	0.407	0.385	1.160

† The atomic parameters were newly refined by Kusaka (1999) with anisotropy for the thermal displacement factors.

The variation of the Ca/Sr—O(2)^{ii} bond, being practically negligible, should result from 'in-phase' shifts of these two atoms. Out-of-phase shifts of the pair Ca/Sr and O(3)^{i} or O(3)^{iii} may be related to the displacement of Ca/Sr from the center of the pentagonal channel (Fig. 1). The variations of the bond lengths Ca/Sr—O(3)^{i}/O(3)^{iii}, being longer than Ca/Sr—O(2)^{i}/O(2)^{iii}, are illustrated in Fig. 6 as functions of (t_1, t_2). In the area outlined by the loops at 2.816 Å, these two bonds are longer than the other Ca/Sr—O bonds (see Table 5). If we assume that 2.816 Å is the maximum distance for the O atoms neighboring Ca/Sr, then the coordination number of Ca/Sr decreases from eight to seven in the areas inside the loops in Fig. 6. Since these areas in both diagrams do not overlap with each other, the sixfold coordination of Ca found in $Ca_2CoSi_2O_7$ and $Ca_2(Mg_{0.55},Fe_{0.45})Si_2O_7$ (Kusaka *et al.*, 1998) is not formed in the present material. Examination of bond distribution throughout the $(Sr_{0.13}Ca_{0.87})_2CoSi_2O_7$ crystal shows that the eightfold coordinated polyhedra take 66% of the whole Ca/Sr—O polyhedra in the structure and the remainder 34% are sevenfold.

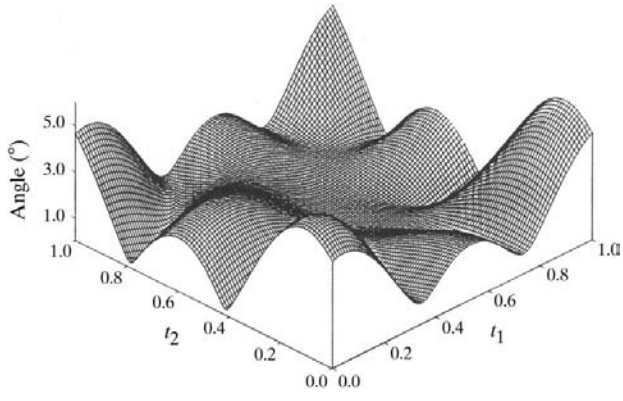

Figure 5
Rotation angles of CoO_4 tetrahedra around ⟨001⟩. The angles correspond to derivation from the angle in the basic structure.

The CoO_4 and SiO_4 tetrahedra show dissimilar variations of the interatomic distances Co—O, Si—O and O—O, and the tetrahedral angles (Table 5). These features demonstrate that distortion of the tetrahedra is induced and it is larger in SiO_4. Variations of the tetrahedral angles in CoO_4 as functions of the parameter t_1 at the section t_2 = 0 are presented in Fig. 7. The angles O(3)^{i}—Co—O(3)^{vii} and O(3)^{v}—Co—O(3)^{vi} of CoO_4 tetrahedra change in-phase with each other and out-of-phase with the remaining angles. In the area where the O(3)^{i}—Co—O(3)^{vii} and O(3)^{v}—Co—O(3)^{vi} angles are large, the lengths of the edges O(3)^{i}—O(3)^{vii} and O(3)^{v}—O(3)^{vi} parallel to (001) increase, but the lengths of the remaining four edges decrease (Fig. 8). As was found in the relative åkermanite $Ca_2(Mg_{0.55},Fe_{0.45})Si_2O_7$ (Kusaka *et al.*, 1998), this is an indication of the flattening of CoO_4 in the (001) plane. The edges of the CoO_4 tetrahedra show opposite variations around (0,1/2), (1/2,0), (1,1/2) and (1/2,1): shortening of the edges parallel to (001) and elongation of the others indicate a swell of the tetrahedron along [001]. By comparing the (t_1, t_2) area in Figs. 8 and 5 we can find that both flattened and swollen CoO_4 tetrahedra are largely rotated. Comparison of Fig. 8 with Fig. 6 shows that the areas of the flattened CoO_4 correspond to the areas of longer Ca/Sr—O(3)^{i} bonds and those of the swollen tetrahedra correspond to the areas of longer Ca/Sr—O(3)^{iii} bonds. To study the influence of the distortion of CoO_4 tetrahedra on interlayer *A* atoms, the variation in Ca/Sr—Ca/Sr distances surrounding the CoO_4 tetrahedra was evaluated against the (t_1, t_2) phase factors (Fig. 9). Two regions can be

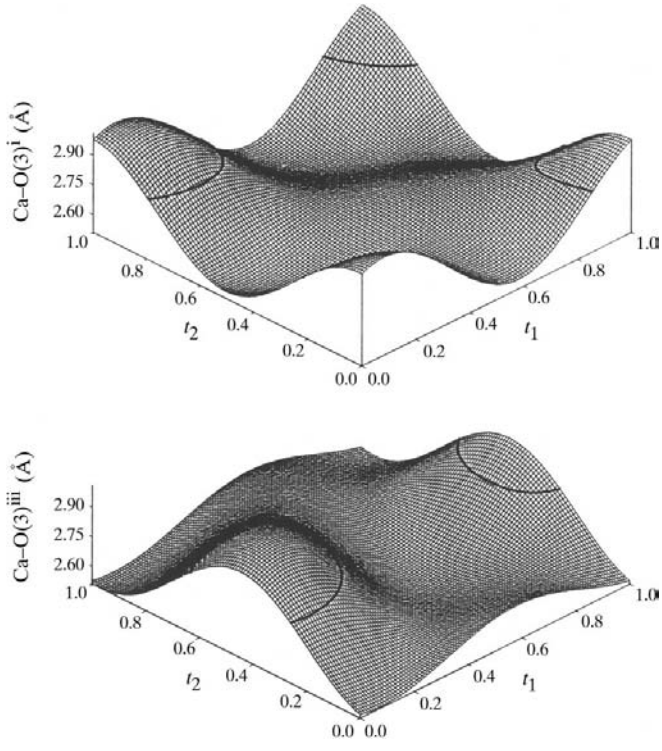

Figure 6
Variations of the Ca—O(3)^{i} and Ca—O(3)^{iii} bond lengths with t_1, t_2 parameters. The contours equal to 2.816 Å are shown. Symmetry codes are shown in Table 5.

discerned: in the first, at around (0,0), (1,0), (0,1), (1,1), the interlayer cation distances are relatively wide, but in the second region at around (0,1/2), (1/2,0), (1,1/2), (1/2,1), the Ca/Sr—Ca/Sr distances are close. The variation of Ca/Sr—Ca/Sr distances is from 4.02 to 4.32 Å and is correlated with a change in edges of the CoO_4 tetrahedra in the following manner: the Ca/Sr—Ca/Sr distances are large around the flattened tetrahedra and are shorter around the swollen ones (see Figs. 8 and 9).

4.3. Comparison of $(Sr_{0.13}Ca_{0.87})_2CoSi_2O_7$ and $Ca_2CoSi_2O_7$ structures

Since the present structure contains two characteristic features, the ordering of the atoms at the *A* site and the absence of sixfold coordination of the *A*-site cation which was found in $Ca_2CoSi_2O_7$ (Hagiya *et al.*, 1993), both structures were compared based on the crystal chemical viewpoints in order to determine the effects of substitution on their modulation. The wavelength of modulation in $Ca_2CoSi_2O_7$ [λ = 19.04 (1) Å] is shorter than that of $(Sr_{0.13}Ca_{0.87})_2CoSi_2O_7$ [λ = 19.41 (3) Å], but the amplitudes of the modulation waves of the former are larger than those of the latter (Table 5 in Hagiya *et al.*, 1993). Therefore, the displacement range of the atoms (Table 6*b*) and the variation of the interatomic distances (Table 7) in $Ca_2CoSi_2O_7$ are larger than those in the present material.

Wide ranges in values are noticed for the Ca—O bonds [Ca—O(2)^{i}, Ca—O(2)^{iii}, Ca—O(3)^{i} and Ca—O(3)^{iii}] and, moreover, the set of bond lengths Ca—O(2)^{i} and Ca—O(3)^{i} (Figs. 10*a* and *c*), and that of the other two lengths Ca—O(2)^{iii} and Ca—O(3)^{iii} (Figs. 10*b* and *d*) individually vary in phase. The contours are drawn at the same level (2.816 Å) as those in Fig. 6. The areas surrounded with the contours in the Ca—O(2)^{i} diagram overlap with similar ones in the Ca—O(3)^{i} diagram, and the same situation is realised in the Ca—O(2)^{iii} and Ca—O(3)^{iii} diagrams. The Ca atoms are coordinated with six O atoms in the overlapped areas, but those in the remaining areas enclosed with contours are coordinated with the seven nearest O atoms. The bond distributions of Ca—O polyhedra throughout the crystal show that $Ca_2CoSi_2O_7$

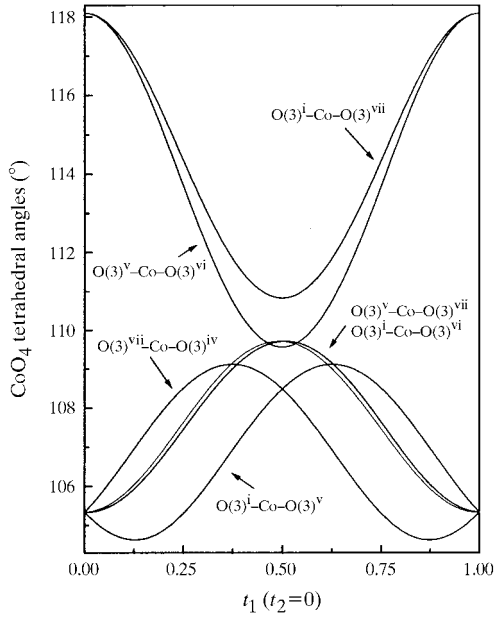

Figure 7
Variations of O—Co—O angles of CoO_4 tetrahedra as functions of the internal parameter t_1 (t_2 = 0). The notations of the atoms are given in Fig. 1.

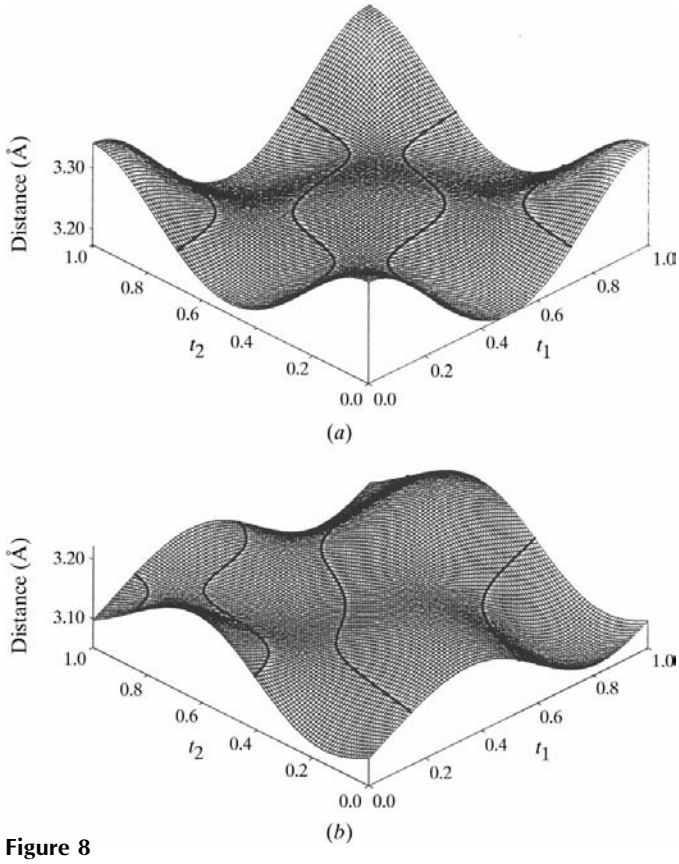

Figure 8
Variations of CoO_4 tetrahedral edge lengths as functions of (t_1, t_2). (*a*) Edges almost parallel to (001): O(3)^{i}—O(3)^{vii} and O(3)^{v}—O(3)^{vi}; (*b*) O(3)^{v}—O(3)^{i} and O(3)^{vii}—O(3)^{vi} edges. Symmetry codes are shown in Table 5.

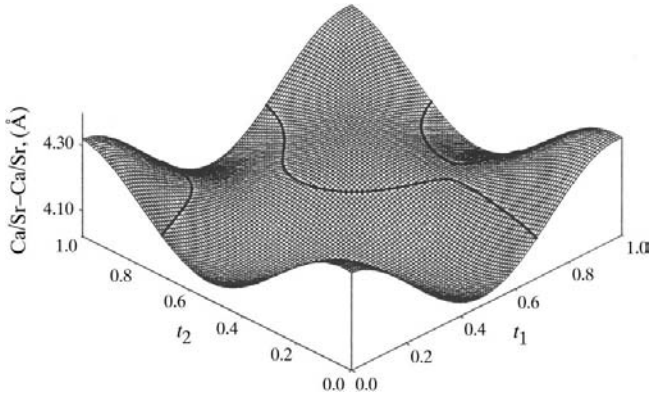

Figure 9
Ca/Sr—Ca/Sr distances close to the CoO_4 tetrahedron as functions of the phases (t_1, t_2). Contour lines corresponding to the mean value 4.145 Å are drawn.

Table 7
The interatomic distances (Å) and tetrahedral angles (°) of $Ca_2CoSi_2O_7$.

The atomic parameters were newly refined by Kusaka (1999) with anisotropy for the thermal displacement factors.

		Modulated structure		
	Basic structure	Minimal	Maximal	Variation
Ca—O polyhedra				
Ca—O(1)^{i}	2.499 (2)	2.312 (3)	2.757 (4)	0.445 (6)
Ca—O(2)^{ii}	2.455 (2)	2.422 (4)	2.507 (4)	0.085 (5)
Ca—O(2)^{i,iii}	2.722 (2)	2.358 (4)	3.142 (5)	0.784 (6)
Ca—O(3)^{ii,iv}	2.423 (2)	2.276 (4)	2.615 (5)	0.339 (6)
Ca—O(3)^{i,iii}	2.681 (2)	2.255 (2)	3.745 (6)	1.490 (8)
Average length	2.576 (2)	2.314 (5)	3.034 (6)	0.720 (8)
CoO_4 tetrahedra				
Co—O(3)^{i,v,vi,vii}	1.940 (2)	1.908 (4)	1.999 (4)	0.091 (5)
O(3)$^{i(vii)}$—O(3)$^{v,vi(v,vi)}$	3.139 (3)	2.967 (4)	3.293 (6)	0.326 (4)
O(3)$^{i(v)}$—O(3)$^{vii(vi)}$	3.225 (3)	3.141 (5)	3.648 (4)	0.507 (6)
O(3)$^{i(vii)}$—Co—O(3)$^{v,vi(v,vi)}$	108.00 (8)	99.42 (11)	113.82 (9)	14.40 (14)
O(3)$^{i(v)}$—Co—O(3)$^{vii(vi)}$	112.45 (7)	107.57 (12)	131.88 (10)	24.31 (15)
SiO_4 tetrahedra				
Si—O(1)^{ii}	1.648 (1)	1.628 (3)	1.696 (4)	0.068 (5)
Si—O(2)^{viii}	1.589 (2)	1.593 (5)	1.616 (6)	0.023 (4)
Si—O(3)^{ii,iv}	1.618 (2)	1.585 (4)	1.686 (4)	0.101 (5)
O(1)—O(2)^{viii}	2.676 (3)	2.645 (4)	2.734 (5)	0.089 (6)
O(1)—O(3)^{ii,iv}	2.522 (2)	2.503 (5)	2.696 (4)	0.193 (5)
O(2)^{viii}—O(3)^{ii,iv}	2.750 (3)	2.718 (6)	2.782 (5)	0.064 (6)
O(3)—O(3)^{iv}	2.557 (3)	2.495 (6)	2.639 (4)	0.144 (7)
O(1)—Si —O(2)^{viii}	111.50 (8)	110.16 (8)	111.69 (10)	1.53 (10)
O(1)—Si —O(3)^{ii,iv}	101.14 (9)	98.49 (10)	108.36 (11)	9.87 (11)
O(2)^{viii}—Si —O(3)^{ii,iv}	118.04 (8)	112.96 (9)	118.97 (11)	6.01 (9)
O(3)—Si —O(3)^{iv}	104.44 (9)	102.98 (11)	106.41 (8)	3.43 (11)

Symmetry codes: see Table 5.

consists of 35.5% eightfold, 36% sevenfold and 28.5% sixfold coordinated Ca—O polyhedra.

In $Ca_2CoSi_2O_7$ the twisting angles of the Si_2O_7 dimer throughout the structure vary ±27.03° from the angle in the basic structure (119.32°) and the rotation angles of CoO_4 around ⟨001⟩ vary 21.02° from the positions in the basic structure. The Ca—Ca distances surrounding the CoO_4 tetrahedra change from 3.770 (2) to 4.666 (2) Å with the average distance 4.124 (2) Å. The range of Ca—Ca distances, the twisting angles of Si_2O_7 and the rotation angles of CoO_4 in $(Sr_{0.13}Ca_{0.87})_2CoSi_2O_7$ are smaller than those in $Ca_2CoSi_2O_7$ and the reduction in the variation may be derived through the substitution of Ca by Sr.

The sum of the bond valence of each cation in both structures was evaluated in order to esti-

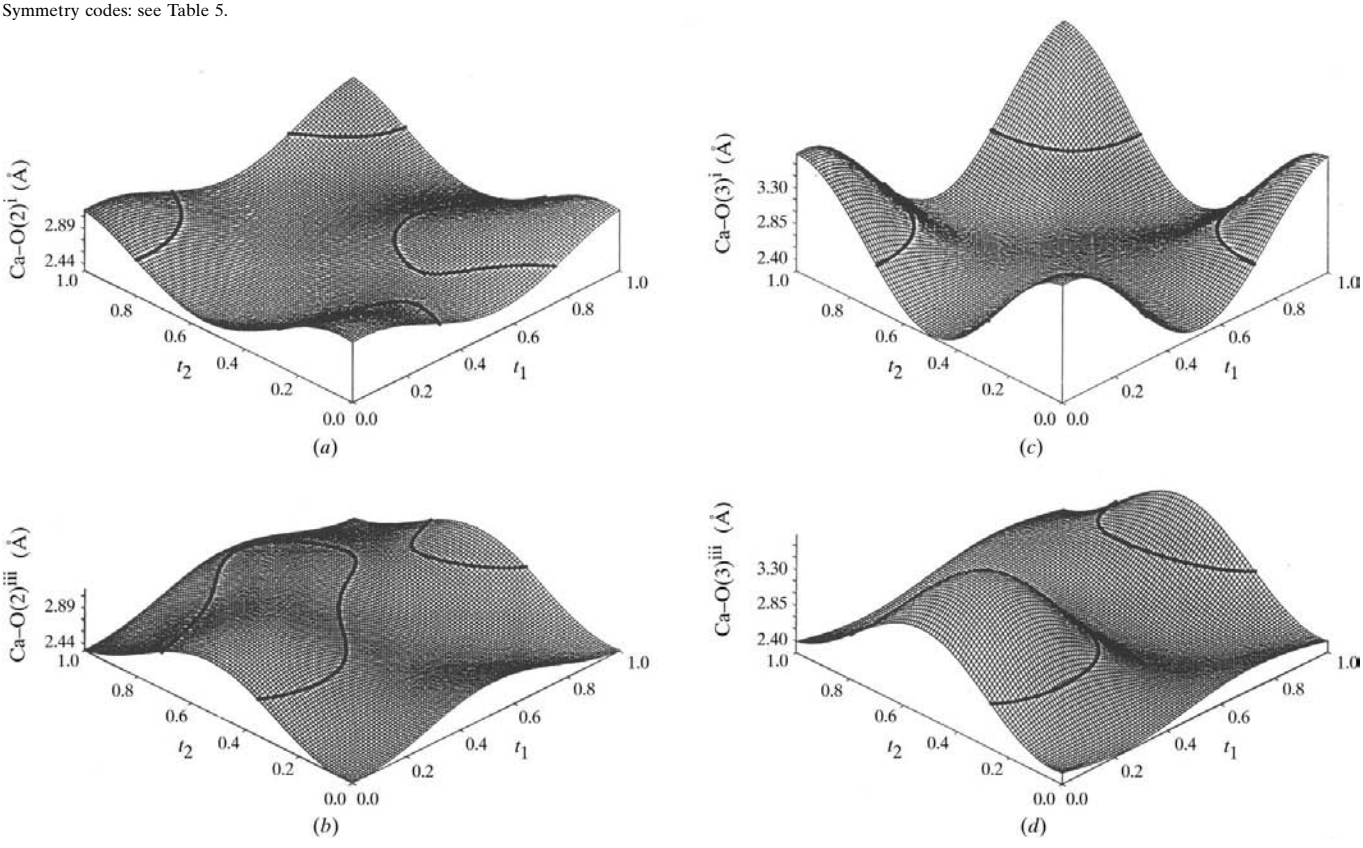

Figure 10
Variation of the Ca—O(2)^{i}, Ca—O(2)^{iii} and Ca—O(3)^{i}, Ca—O(3)^{iii} bond lengths in $Ca_2CoSi_2O_7$. The contours correspond to 2.816 Å. Symmetry codes are shown in Table 5.

mate the fit of the coordination polyhedra around the atoms in the structures using the method presented by Brown (1992) and the valence parameters given by Brown & Altermatt (1985). The values are listed in Table 8. The values for Sr/Ca in $(Sr_{0.13}Ca_{0.87})_2CoSi_2O_7$ were calculated by summing up the bond valence of Sr and Ca in the ratio of each occupancy. The bond-valence sums of the Si and Co cations calculated with the coordinates of both the basic structures virtually agree with the expected formal charges of the atoms, except the values for the *A*-site atoms which are remarkably lower than their formal charges. The low values suggest that the interstices of the coordination polyhedra are too loose for the *A* atoms. The values for all cations in the modulated structures vary markedly, as indicated in Table 8 and Fig. 11, but their mean values are closer to the expected values than the values of the basic structures. The variation of the bond-valence sum for Si is very high in $Ca_2CoSi_2O_7$, while the value is much lower in $(Sr_{0.13}Ca_{0.87})_2CoSi_2O_7$. A similar but moderate tendency is also found for Co in both materials. However, the variation of the bond-valence sums of the *A*-site cations in both structures indicates opposite behavior, that is, the variation of the values is larger in $(Sr_{0.13}Ca_{0.87})_2CoSi_2O_7$ and smaller in $Ca_2CoSi_2O_7$. The areas with high bond-valence sums of Ca in $Ca_2CoSi_2O_7$ (Fig. 11*a*) generally correspond to the areas of low-coordinated Ca—O polyhedra given in Fig. 10. The bond-valence sums of Co and Si (Figs. 11*b* and *c*) indicate an approximate inverse correlation with those of Ca: the sums indicate that the Co and Si tetrahedra are much expanded in the areas corre-

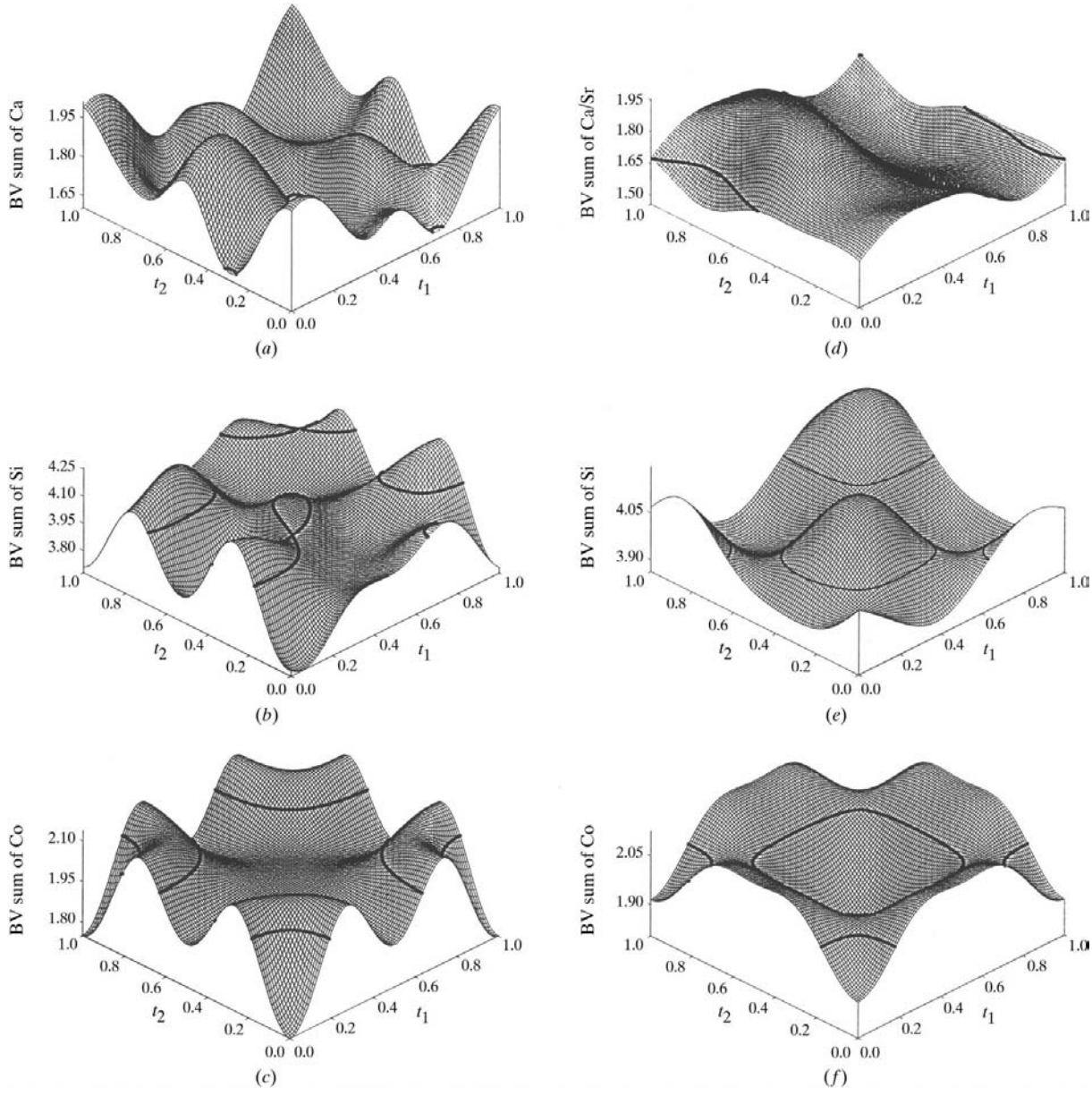

Figure 11
(*a*, *b*, *c*) Bond-valence sums of the Ca, Co, Si cations in $Ca_2CoSi_2O_7$ as functions of t_1, t_2. The contours correspond to the bond-valence sums in the basic structure (see Table 8*a*). (*d*, *e*, *f*) Bond-valence sums of the Ca/Sr, Co and Si cations in $(Sr_{0.13}Ca_{0.87})_2CoSi_2O_7$ as functions of t_1, t_2. The contours correspond to the bond-valence sums in the basic structure (see Table 8*b*).

Table 8
Cation bond-valence sums.

		Modulated structure			
	Basic structure	Mean value	Minimal	Maximal	Variation
(*a*) $Ca_2CoSi_2O_7$					
Ca	1.637	1.766	1.604	2.014	0.410
Co	2.048	2.011	1.752	2.140	0.388
Si	4.071	3.980	3.677	4.258	0.581
(*b*) $(Sr_{0.13}Ca_{0.87})_2CoSi_2O_7$					
Sr/Ca	1.675	1.698	1.460	1.958	0.498
Co	2.028	2.020	1.804	2.128	0.324
Si	4.024	4.013	3.862	4.199	0.337

sponding to the low-coordinated Ca—O polyhedra, but they are contracted in the areas of the eight-coordinated Ca.

Although the displacement pictures of the atoms are similar in both structures, the magnitudes of the displacement and the variation of the bond-valence sums for Si and Co are fairly reduced in the present material (Table 8*b*). Especially the distributions of the bond-valence sums of the *A*-site atom and Si in $(Sr_{0.13}Ca_{0.87})_2CoSi_2O_7$ (Figs. 11*d* and *e*) are quite different from those in $Ca_2CoSi_2O_7$: the former are smooth ones, while the latter are rough. A similarity is noticed between the distribution of the bond-valence sums of Ca/Sr and that of the occupancy of Sr at the *A* site, that is, the area with a high concentration of Sr (Fig. 2) corresponds to the area of high bond-valence sums (Fig. 11*d*) where the values are closer to the formal valence than the remaining area. This suggests that the substitution of Ca by Sr should cause a relaxation in the distortion of the structure induced by stronger bonds of Ca and would be reflected in the reduced values of the bond-valence sums at the Si site. The inverse correlation between the bond-valence sums of the *A*-site atom and Co, Si found in $Ca_2CoSi_2O_7$ is not detected in $(Sr_{0.13}Ca_{0.87})_2CoSi_2O_7$.

Since the effects of substitution at the *A*-site mentioned above are similar to the usual temperature behaviour of modulation in structures such as A_2BX_4 compounds (Cummins, 1990), shortening of the wavelength and increase of the amplitudes of the modulation waves will take place in $(Sr_{0.13}Ca_{0.87})_2CoSi_2O_7$ at a temperature lower than room temperature and the smooth distribution of the bond-valence sums of Sr/Ca will therefore be rougher than the present results. No modulated structure has so far been discovered in the $(Sr_xCa_{1-x})_2CoSi_2O_7$ solid solution with Sr content $x > 0.3$ at room temperature (Iishi *et al.*, 1990), but the presence of modulated structures may be predicted based on the above consideration in the compounds with higher Sr content than 0.3 at temperatures lower than room temperature.

The authors thank Y. Tani for the measurements of the diffraction data and the preliminary computation, Dr V. Petricek for advice during the refinement using *JANA*. The authors (BB and MO) would like to express their gratitude to the Japan Society for the Promotion of Science for the financial support. The work was also financially supported in part by a Grant-in-Aid for Scientific Research (B) (No. 07454135) from the Ministry of Education, Science and Culture, Japan, which are gratefully acknowledged.

References

Armbruster, T., Röthlisberger, F. & Seifert, F. (1990). *Am. Mineral.* **75**, 847–858.
Becker, P. & Coppens, P. (1974). *Acta Cryst.* A**30**, 129–147.
Brown, I. D. (1992). *Acta Cryst.* B**48**, 553–572.
Brown, I. D. & Altermatt, D. (1985). *Acta Cryst.* B**41**, 244–247.
Cummins, H. Z. (1990). *Phys. Rep.* **185**, 211–409.
Hagiya, K., Ohmasa, M. & Iishi, K. (1993). *Acta Cryst.* B**49**, 172–179.
Hemingway, B. S., Evans, H. T. Jr, Nord, G. L. Jr, Haselton, H. T. Jr, Robie, R. A. & McGee, J. J. (1986). *Can. Mineral.* **24**, 425–434.
Iishi, K., Fujino, K. & Furukawa, Y. (1990). *Phys. Chem. Miner.* **17**, 467–471.
Iishi, K., Hagiya, K. & Ohmasa, M. (1994). *Phys. Chem. Miner.* **21**, 6–11.
Kusaka, K. (1999). Ph.D. thesis. Himeji Institute of Technology, Japan.
Kusaka, K., Ohmasa, M., Hagiya, K., Iishi, K. & Haga, N. (1998). *Mineral. J.* **20**, 47–58.
Petricek, V. & Dusek, M. (1998). *JANA*98. Institute of Physics, Academy of Sciences, Praha, Czech Republic.
Riester, M. & Böhm, H. (1997). *Z. Kristallogr.* **212**, 506–509.
Röthlisberger, F., Seifert, F. & Czank, M. (1990). *Eur. J. Miner.* **2**, 585–594.
Seifert, F., Czank, M., Simons, B. & Schmahl, W. (1987). *Phys. Chem. Miner.* **14**, 26–35.
Shannon, R. D. (1976). *Acta Cryst.* A**32**, 751–767.
Smith, J. V. (1953). *Am. Mineral.* **38**, 643–661.
Wolff, P. M. de, Janssen, T. & Janner, A. (1981). *Acta Cryst.* A**37**, 625–636.